Conf-950167--4

DISTRIBUTION OF THIS DOCUMENT IS UNLIMITED

MASTER

SAND94-2784C

Auger Rates in Mid-IR InAsSb Laser Structures

H. P. Hjalmarson and S. R. Kurtz
Sandia National Laboratories, Albuquerque, NM 87185-0603

Abstract

Auger rates are calculated for three InAsSb mid-infrared laser structures as a function of temperature. Compressive strain in the quantum wells reduces the mass of the holes; it is shown that this leads to a reduction in the Auger rate compared with an unstrained quantum well. The Auger rates for these structures are similar primarily due to their similar bandgap energies.

1. Introduction

Auger recombination is often the dominant non-radiative mechanism in narrow gap semiconductors used for infrared (IR) applications. In this work we compute the Auger rate for InAsSb optically active layers being fabricated as light-emitting diodes (LED's) and lasers.[1][2] The guiding motivation is the use of bandgap engineering to reduce the Auger rates.[3] The resultant bandstructure is highly non-parabolic which led to our development of a new theoretical technique to explore this issue. The calculation involves computation of *k.p* energies and wavefunctions for the strained quantum well structure. This information is used in the calculation of Auger rates and lifetimes as a function of doping and injected carrier density. In this paper we use this calculation to define two design rules for these structures. One, we show that a reduction of the hole transverse mass reduces the Auger rate dramatically. Two, we define the barrier thickness which is sufficient to minimize the rate due to coupling between wells.

2. Formalism for Auger rates

The 2D Auger rate calculation is similar to earlier work on bulk 3D structures.[4] The earliest work on 2D systems focused on quantum well laser structures.[5, 6] More recent work has focused on quantum well superlattices.[7] Fermi's Golden Rule defines the Auger rate

$$1/\tau = \frac{2\pi}{\hbar} \sum_{ii'ff'} |V_{ii'ff'}|^2 f_i f_{i'} (1-f_f)(1-f_{f'}) \delta(E_i + E_{i'} - E_f - E_{f'}) \tag{1}$$

in terms of Fermi functions $f_i \equiv f((E_i - E_{F_i})/k_B T)$ and matrix elements

$$V_{ii'ff'} = \frac{e^2}{4\pi\epsilon} \int d^3r \int d^3r' \frac{\Psi_i(r)\Psi_{i'}(r')\Psi_f(r)\Psi_{f'}(r')}{|r-r'|}. \tag{2}$$

The wavefunctions

$$\Psi_i(r) \equiv \Psi_{n_i k_i}(r) = \sum_{m_i} \Phi_{n_i k_i m_i}(z) u_{m_i}(r) \exp(i\mathbf{k}_i \mathbf{r}) \tag{3}$$

are written in terms of an envelope function $\Phi(r)$ and the Bloch functions $u(r)$. These wavefunctions and the energies E_{nk} are obtained from a strained k.p calculation.[8]

DISCLAIMER

This report was prepared as an account of work sponsored by an agency of the United States Government. Neither the United States Government nor any agency thereof, nor any of their employees, makes any warranty, express or implied, or assumes any legal liability or responsibility for the accuracy, completeness, or usefulness of any information, apparatus, product, or process disclosed, or represents that its use would not infringe privately owned rights. Reference herein to any specific commercial product, process, or service by trade name, trademark, manufacturer, or otherwise does not necessarily constitute or imply its endorsement, recommendation, or favoring by the United States Government or any agency thereof. The views and opinions of authors expressed herein do not necessarily state or reflect those of the United States Government or any agency thereof.

DISCLAIMER

Portions of this document may be illegible in electronic image products. Images are produced from the best available original document.

By analogy to the Beattie-Landsberg expression for 3D systems, the 2D Auger lifetime τ for an n-doped structure can be written as

$$1/\tau = \frac{(n_0 + p_0 + \nu)(n_0 + \nu)}{n_i^2}\frac{1}{\tau_i} \tag{4}$$

in terms of the intrinsic lifetime τ_i defined by

$$1/\tau_i = 1.65 \times 10^{17} \frac{F(G_T)^2}{\kappa^2 (E_G/k_B T)(1 + 2m_c/m_v)(m_c/m_0)} \exp(-E_T/k_B T) \tag{5}$$

in which E_T is the threshold energy, the energy which must be exceeded for an Auger transition (it is determined by energy and momentum conservation). The transition assumed involves two electrons in the conduction (C) sub-band which scatter to a conduction sub-band and a valence (V) sub-band (a CCCV transition). In these expressions, ν is the injected carrier density; n_0 and p_0 are the electron and hole equilibrium concentrations, respectively. The other quantities are the dielectric constant κ, the conduction band effective mass m_c, the valence band effective mass m_v, the bandgap E_g, and the temperature T. Only one valence and one conduction sub-band are assumed for this simplified, heuristic expression. A similar expression can be written for a VVVC transition. The calculations to be described involve a generalization of Eq. (4) in which the form factor is computed by a probablistic average over k-vectors corresponding to the threshold energy.

The form factor

$$F(G) = \sum_{m,m'} \int dz \int dz' \varphi_{im}(z)\varphi_{i'm'}(z')\varphi_{fm}(z)\varphi_{f'm'}(z') \exp(-G|z - z'|) \tag{6}$$

represents the overlap of the initial (i and i') state and final (f and f') state wavefunctions. For a superlattice of quantum wells the form factor can be rewritten in terms of an integration over the periodic function times an exponential phase factor:

$$\varphi(z) = \chi(z) \exp(iqz). \tag{7}$$

The form factor also includes the Coulomb interaction, responsible for Auger transitions, through the momentum transfer G_T. This quantity controls the range

$$R \approx \frac{1}{G_T} \tag{8}$$

of the Coulomb potential. If G is small, the range is large leading to large contributions to the rate. The transverse and longitudinal contributions enter separately. A $1/G_T^2$ term describes the contributions from within each well (this term does not appear directly in the final expression). The form factor term $\exp(-G_T L)$ describes the contribution from adjacent wells in terms of the superlattice periodicity L.

By inspection, the Auger rate can be reduced by increasing the threshold energy. In the most simple effective mass approximation the activation energy

$$\Delta E \equiv E_T - E_G = \frac{m_c}{m_v + m_c} E_G \tag{9}$$

in which E_G is the bandgap energy. This observation immediately leads to the use of strain to reduce the transverse hole mass thereby reducing the Auger rate.

Another design rule follows from the strength of the interaction in terms of the threshold momentum transfer G_T. In the effective mass approximation, the momentum transfer depends on bandgap and effective mass in a simple way:

$$G_T^2 = \frac{m_v + m_c}{m_v + 2m_c} \frac{2m_c}{\hbar^2} E_g \tag{10}$$

Equation (6) leads directly to the second design rule: Choose the barrier thickness such that $G_T L < 1$. If L exceeds the range $R = 1/G_T$, then carriers in adjacent wells cannot contribute to the Auger rate. In other words, the quantum wells are decoupled with no coherent non-radiative transitions due to the long-range Coulomb potential.

DISTRIBUTION OF THIS DOCUMENT IS UNLIMITED

The Auger calculations involve separate bandstructure and rate calculations. The $k \cdot p$ bandstructure is computed for each strained structure. The energies, wavefunctions, and dipole matrix elements are tabulated and used as input for the rate calculations. Due to the importance of strain in these structures, both energies and wavefunctions are assumed to be non-parabolic. The wavefunctions enter the calculation through the various form factor approximations. For example, the form factor can be chosen to be a constant to compare with earlier work on 3D systems. [4] Since the wavefunctions depend on spin, both Coulomb and exchange matrix elements can be included directly with no approximations. Screening can also be included.

The calculations can be done for both low and high carrier density limits. These are distinct calculations. The low density limit is useful for materials and doping studies. The high density limit applies to laser structures for which the Auger lifetime and the Auger contribution to the laser threshold current can be evaluated. This calculation requires an estimate of the external mirror losses. Given such an estimate, the total radiated optical power and its spectral dependence can be computed as a function of external electrical power.

To illustrate the design rules we examine the Auger lifetimes as a function of temperature for three proposed laser structures. Materials and electronic information about these structures is tabulated in tables I and II.[9] Because of ambiguity about the k.p parameters for these structures they are approximated by parameters for InAs. Each material is distinguished by its band offset relative to InAs and its band gap. The Luttinger parameters g_1 =3.34, g_2 = -0.23, and g_3 = 0.57; the optical matrix element $V_{opt} = 20.2$ eV.[9]

Figure 1 shows the bandstructure for the InSbAs/InGaAs structure. The bandgap $E_g = 0.329$ eV for this structure. The other structures have similar bandgaps as can be seen in Table II.

We illustrate the first rule which states that a bandgap-engineered reduction in the hole effective mass leads to a reduced Auger rate. Figure 2 shows the Auger lifetime for the InSbAs/InGaAs structure with and without strain for an n-doped sample with $n_0 = 10^{10}$ cm^{-2}. By inspection, the strain increases the Auger lifetime dramatically by a factor of 100. The slope of the lifetime versus 1/T is increased showing that the effect has been to increase the threshold energy. By inspection, the asymptotes at high temperatures are similar. For these calculations and those to be described the CCCH transitions from the $n = 1$ conduction sub-band were computed. The final states considered are the $n = 1, 2$ valence bands as well as the $n = 1, 2$ conduction bands. The calculations involve a generalization of Eq. (4) in which the form factor is computed by a probabilistic average over k-vectors corresponding to the threshold energy.

The Auger lifetimes as a function of temperature for the three structures are compared in Fig. 3. These lifetimes are remarkably similar primarily due to their similar bandgap energies and similar thicknesses. Clearly the lifetime is sensitive to variations in bandgap energy. However, it is also sensitive to quantum well thickness. A thinner well would have a larger Auger rate than a thicker well because of the increased quantum confinement which would lead to an increased form factor. This, of course, assumes other quantities such as the threshold energy are unchanged.

Finally these structures illustrate the second design rule. For each of these structures,

$$G_T \approx 0.02 \frac{2\pi}{a} \tag{11}$$

in terms of the unit cell length a. This leads to a range R which the barrier thickness must exceed. For these structures $R \approx 5$ nm. The barrier of each structure exceeds this range. Because of the resultant insensitivity to barrier thickness, the lifetimes for these structures are similar in spite of the variation in barrier thickness (see Table II). The second design rule would play an important role in structures with InAs/InGaSb superlattices with thin barriers (for example, 3.7 nm).[7] For these structures it has been shown that superlattice mini-band transitions can dominate the Auger rate. [7]

In general, we found the form factor to be very important. Thus it was important to compute the $k.p$ wavefunctions. At the threshold, we find

$$F(G_T)^2 \approx 10^{-4} - 10^{-3} \tag{12}$$

which is approximately $10\times$ smaller than the form factor estimates using simple envelope functions. These $k.p$ form factors differ from more crude approximations in that the parity selection rules obtained from the most simple effective-mass wavefunctions are not valid. These selection rules are broken by inclusion of the dipole matrix element which couples the valence and conduction sub-bands. [10]. Thus

the $n = 2$ conduction and valence sub-bands can contribute to the rate. We find their contributions are comparable to the $n = 1$ sub-bands. The $n = 2$ valence bands contribute due to band filling at high temperature. The $n = 2$ conduction bands contribute as final states because they reduce the threshold energy by the $n = 2$, $n = 1$ band separation. However, we caution that these form factors should be regarded as untested as no independent checks on their accuracy have been completed. Comparisons of the calculated spectra and radiative rates to experimental data will independently test the form factors.[10] For example, the form factors and radiative rates are dependent on the optical matrix element V_{opt}.

Finally, we compare the Auger lifetime with a relative measurement of the lifetime for the InAsSb/InGaAs structure using photoluminescence.[9] We assume the photoluminescence intensity

$$I \approx \frac{1/\tau_r}{1/\tau_r + 1/\tau_{nr}} \tag{13}$$

in which τ_r is the radiative lifetime and τ_{nr} is the non-radiative lifetime. At high temperatures at which the Auger recombination dominates the non-radiative rate, we can assume

$$I \sim \frac{\tau_{nr}}{\tau_r} \tag{14}$$

Under this assumption the intensity is proportional to the Auger lifetime. As shown in Fig. 4, the intensity and the computed Auger lifetime show very good agreement in slope at high temperature. The measured activation energy $\Delta E \approx 0.08$ eV, in good agreement with Eq. 9.[9] Furthermore, we observe that $\tau_r, \tau_{Auger} \sim T$; this common temperature dependence cancels in Eq. 14 producing the nearly ideal Arrhenius behavior shown in Fig. 4. However, this temperature term causes all the lifetime curves (Fig. 2-4) to have pronounced deviations from Arrhenius behavior.

In conclusion, we have shown that bandgap engineering can reduce the Auger rates for mid-IR laser structures. The two design rules state that the hole effective mass must be reduced and the barrier thickness must exceed a critical thickness. Future work will extend these calculation to Auger and optical recombination within laser structures at elevated injected carrier densities which exceed the lasing threshold.

3. Acknowledgments

This work was supported by the US Department of Energy under contract DE-AC04-94AL85000. We thank T. B. Bahder, M. H. Crawford, T. J. Drummond, and Y. Zhang for useful discussions.

References

[1] Kurtz SR, Biefeld R M, Dawson L R, Baucom K C, and Howard A J 1994 Appl. Phys. Lett. **64** 812

[2] Choi H K, Turner G W, and Le H Q (to be published)

[3] Adams A R 1986 Elect. Lett. **22** 249

[4] Beattie A R and Landsberg P T 1959 Proc. Phys Soc. A **249** 16-29

[5] Sugimura A 1983 IEEE J. Quantum Electron. **QE-19** 932

[6] Dutta N K 1983 J. Appl. Phys. **54** 1236

[7] Grein C H, Young P M, and Ehrenreich H 1992 Appl. Phys. Lett. **61** 2905

[8] Bahder T B 1990 Phys. Rev. B **41** 11992

[9] Kurtz S R, Biefeld R M and Dawson L R (accepted for publication, Phys. Rev. B)

[10] Hjalmarson H P, unpublished.

Table I: Material characteristics of laser structures

	Wells			Barriers		
	Material	Thickness (nm)	Strain	Material	Thickness (nm)	Strain
A	$InAs_{0.86}Sb_{0.14}$	9.0	-0.007	$In_{0.87}Ga_{0.13}As$	13.0	0.007
B	$InAs_{0.86}Sb_{0.14}$	9.0	-0.007	$In_{0.9}Al_{0.1}As$	10.0	0.007
C	$InAs_{0.91}Sb_{0.09}$	10.0	-0.0059	InAs	50.0	0.0

Table II: Electronic characteristics of laser structures.

	Name	Gap (eV)	Wells (eV)			Barriers (eV)		
			E_c	E_{hh}	E_{lh}	E_c	E_{hh}	E_{lh}
A	InAsSb/InGaAs	0.329	0.311	0.057	0.003	0.499	-0.055	-0.001
B	InAsSb/InGaAs	0.331	0.311	0.057	0.003	0.569	-0.110	-0.056
C	InAsSb/InAs	0.322	0.350	0.056	0.010	0.42	0.0	0.0

4. Figure Captions

Fig. 1: The k.p bandstructure for the $n = 1, 2, 3$ valence sub-band and $n = 1, 2$ conduction sub-bands of the InAsSb/InGaAs structure. For n-doped samples, the most important transitions involve the $n = 1, 2$ valence and conduction sub-bands.

Fig. 2: Comparison of the Auger lifetime as a function of temperature for the InAsSb/InGaAs structure with and without strain. The reduction of the hole effective mass by strain greatly increases the Auger lifetime.

Fig. 3: Comparsion of the Auger lifetimes as a function of temperature for three different mid-IR laser structures. Due to the similar bandgaps, similar thicknesses, and similar materials, all the lifetimes are similar.

Fig. 4: Comparison of the temperature dependent Auger lifetime with photoluminescence. At high temperature, the photoluminescence has been assumed to be reduced due to Auger recombination. The agreement of the slope of the data with that of the theory sustantiates this assumption.

DISCLAIMER

This report was prepared as an account of work sponsored by an agency of the United States Government. Neither the United States Government nor any agency thereof, nor any of their employees, makes any warranty, express or implied, or assumes any legal liability or responsibility for the accuracy, completeness, or usefulness of any information, apparatus, product, or process disclosed, or represents that its use would not infringe privately owned rights. Reference herein to any specific commercial product, process, or service by trade name, trademark, manufacturer, or otherwise does not necessarily constitute or imply its endorsement, recommendation, or favoring by the United States Government or any agency thereof. The views and opinions of authors expressed herein do not necessarily state or reflect those of the United States Government or any agency thereof.

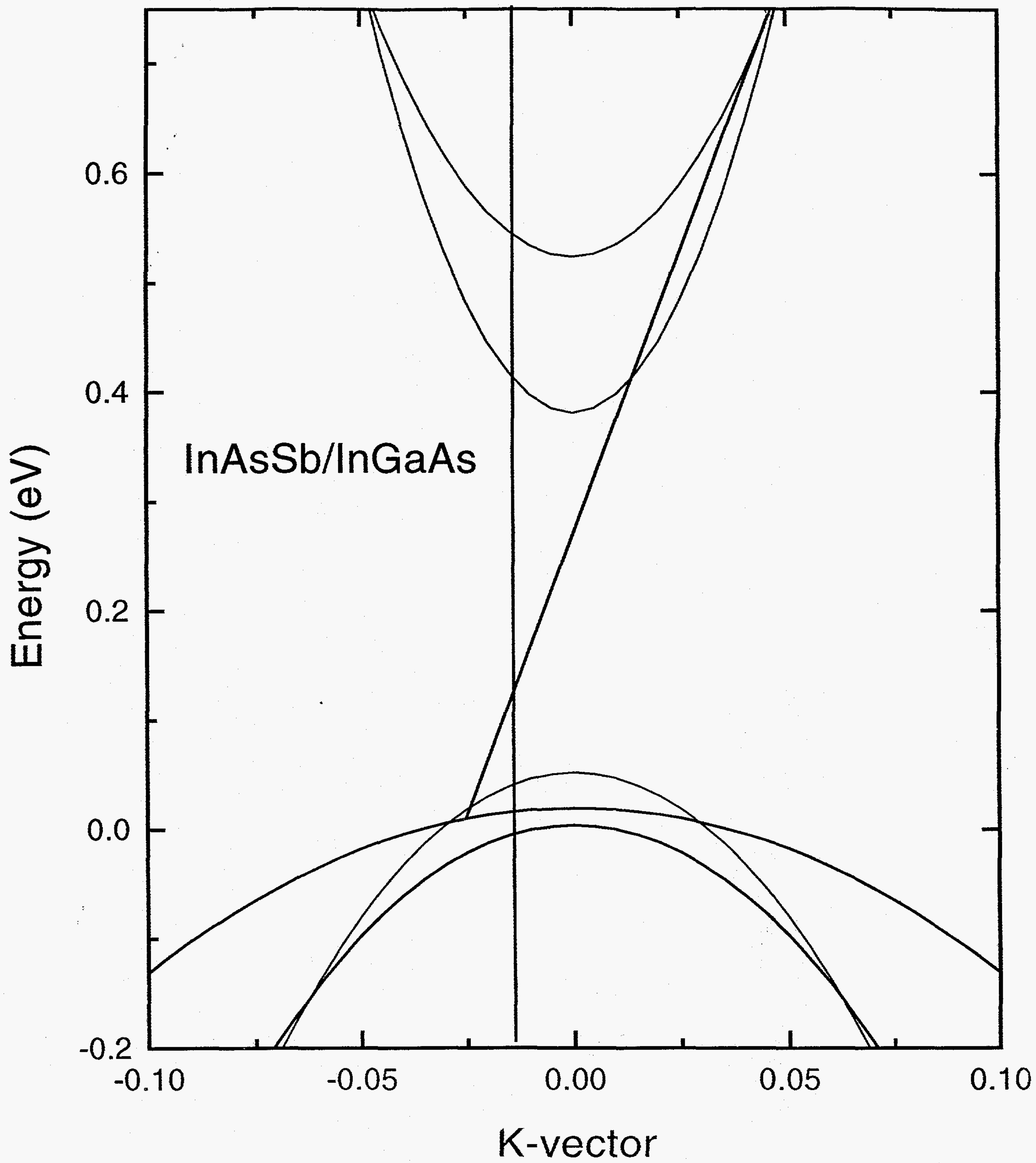

Fig. 1

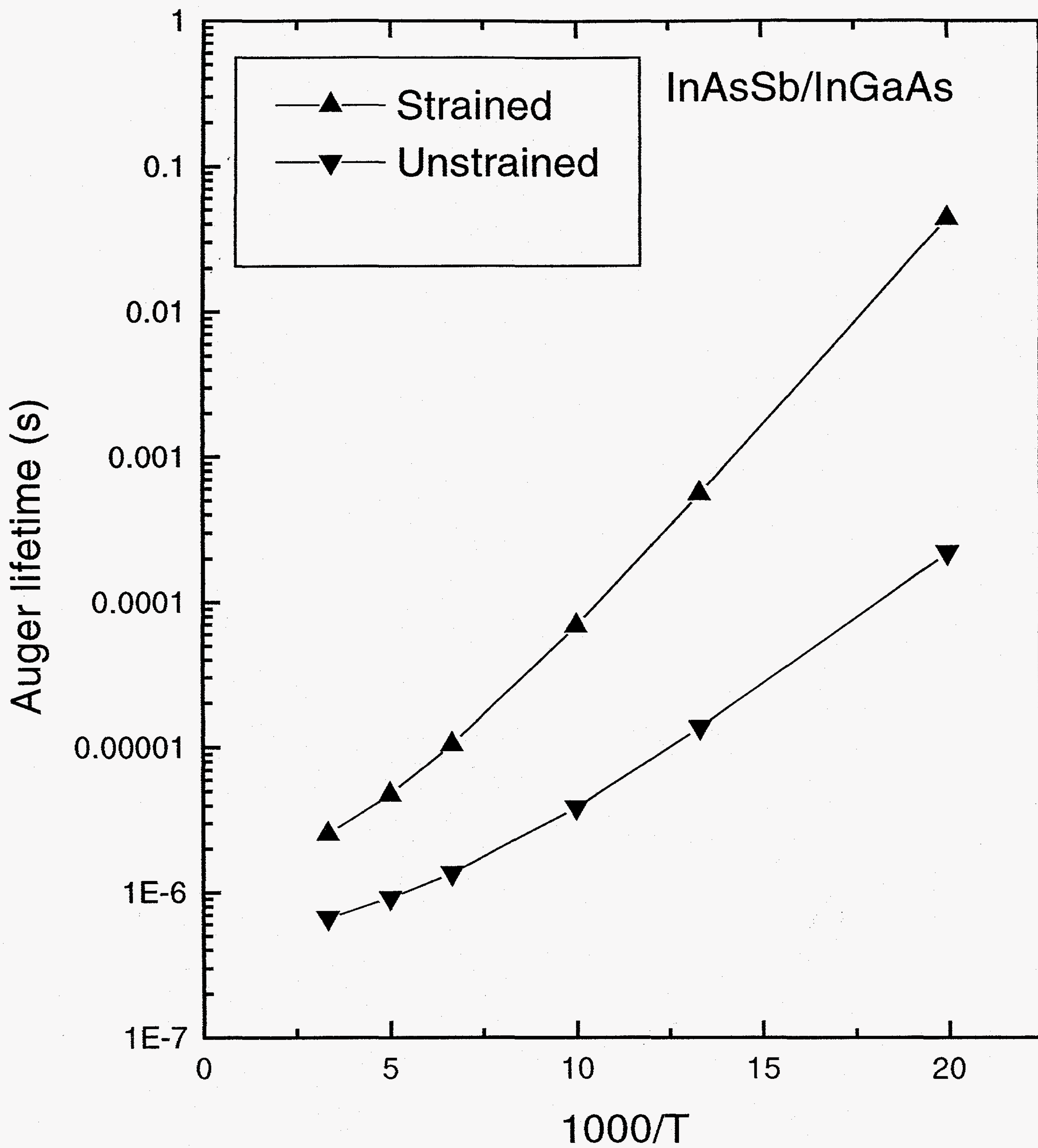

Fig. 2

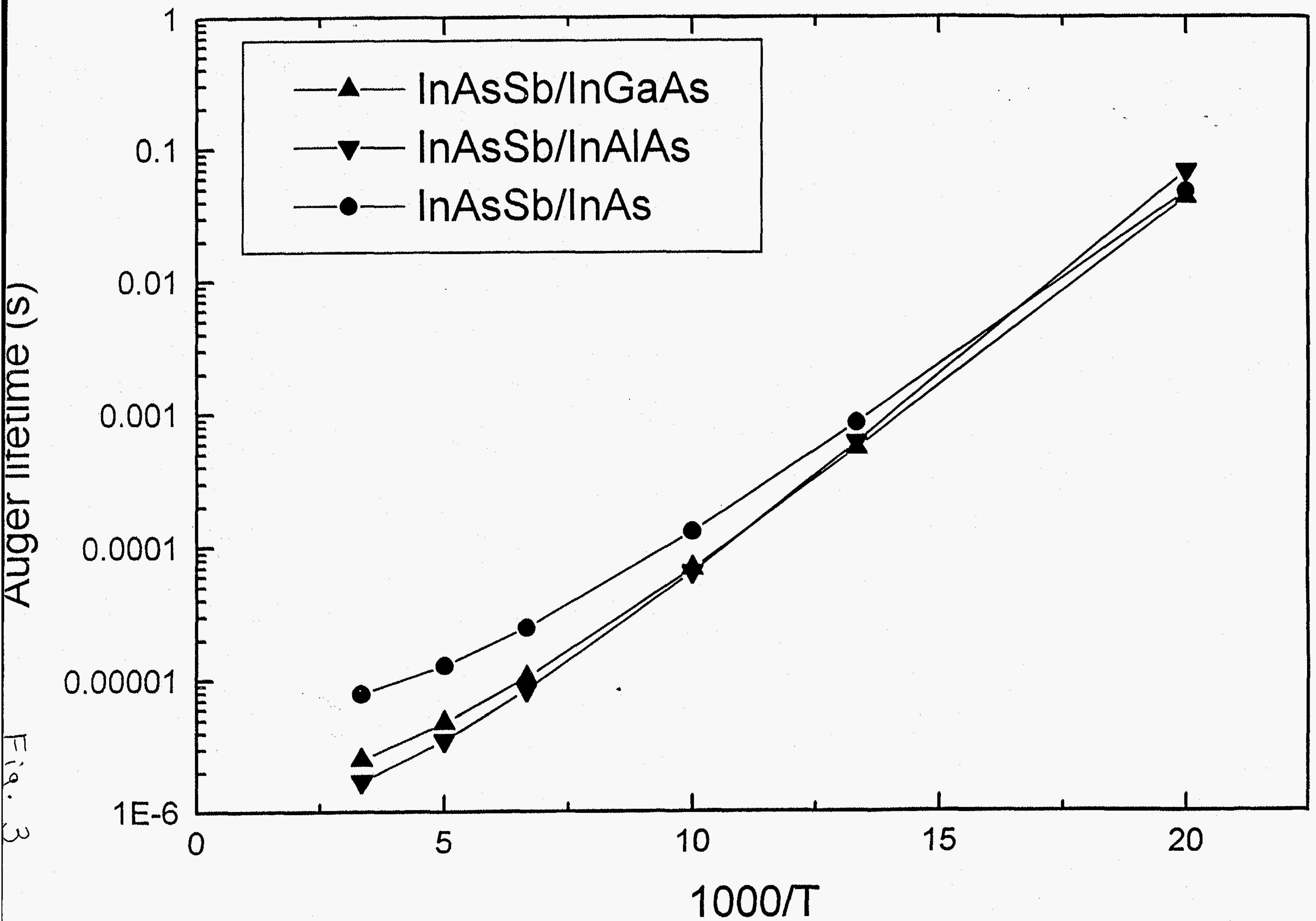

Fig. 3

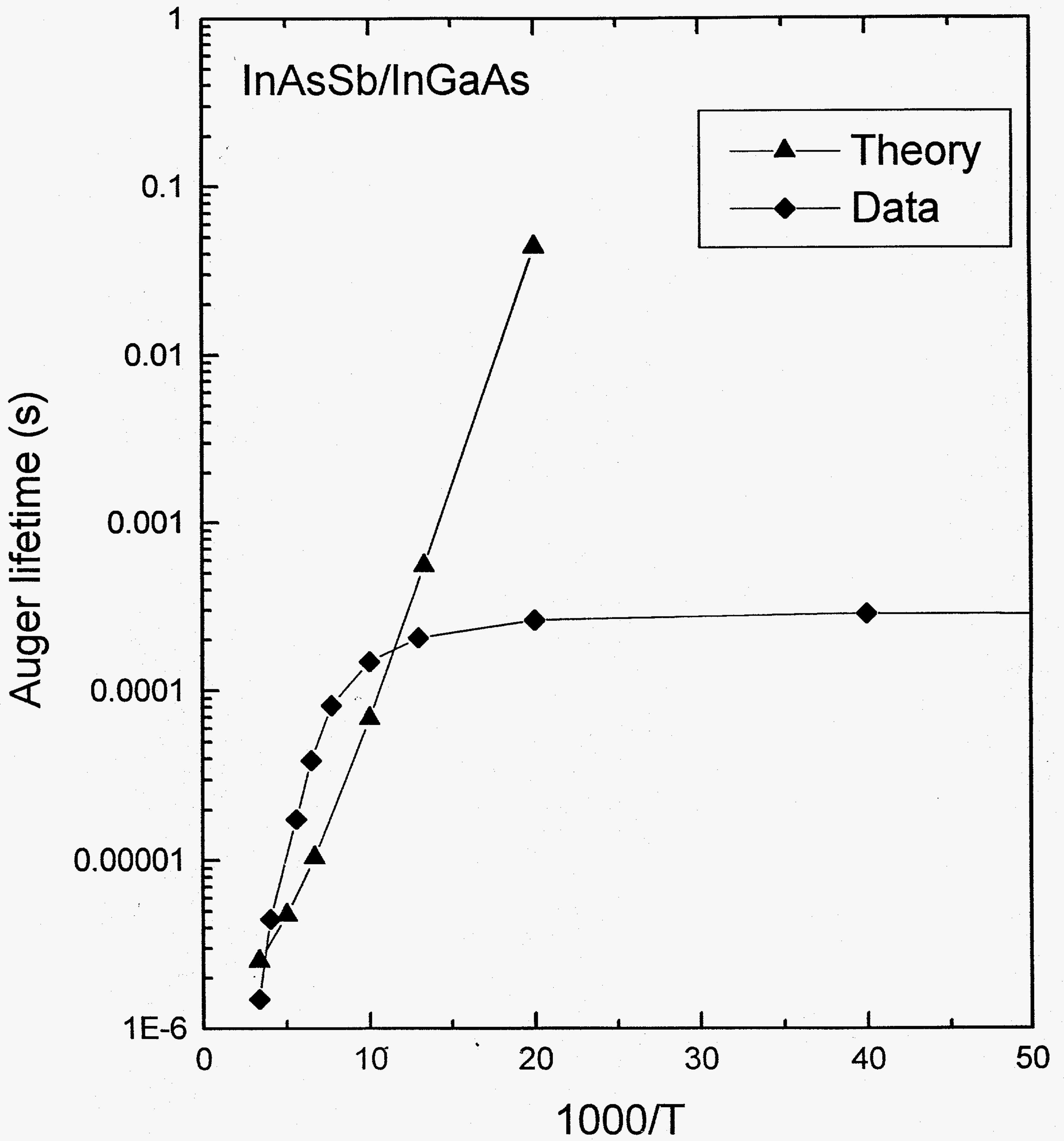

Fig. 4